A study on parametrization of orography-related momentum fluxes in a synoptic-scale NWP model

Laura Rontu[*]

Finnish Meteorological Institute, P.O.Box 503, 00101 Helsinki, Finland

ABSTRACT

In a synoptic-scale atmospheric model, winds and subgrid-scale momentum fluxes are influenced by the properties of the underlying surface. Parametrization schemes have been developed to describe the interactions of the air flow with the rough surface and small- and mesoscale orography. The schemes interact with each other and with the model's dynamical processes. New parametrizations were introduced to the High Resolution Limited Area Model (HIRLAM), to account for the subgrid-scale orography effects. Needed orography parameters were derived from a high-resolution digital elevation data set. A detailed analysis of the momentum fluxes and kinetic energy budget helped to understand the interactions between parametrizations. Mean and root-mean-square error, averaged over all observations and forecasts, did not reveal significant differences between the updated and reference model results. However, more detailed diagnosis of the forecast-observation differences allowed to show that the new parametrizations of mesoscale and small-scale orography lead to more realistic low-level wind distribution.

[*] Corresponding author.

E-mail: laura.rontu@fmi.fi

1   Introduction

Tendencies of the horizontal wind $\vec{v}(x, y, z)$ given by a numerical weather prediction (NWP) model consist of contributions from explicitly resolved dynamics and physical parametrizations of subgrid-scale processes

$$\frac{\partial \vec{v}}{\partial t} = (\frac{\partial \vec{v}}{\partial t})_d + (\frac{\partial \vec{v}}{\partial t})_p \qquad (1)$$

where the indexes d and p refer to dynamics and parametrized physics. In a synoptic-scale model, the dynamical tendency contains terms describing advection, pressure gradient and Coriolis forces. In addition, it is influenced by the accuracy of the numerical schemes, smoothing, boundary relaxation, interpolations etc. The parametrized tendency is due to the divergence of the stress tensor τ_{ij}, which defines the sum of surface forces upon a fluid element. This tendency is conveniently approximated by the vertical divergence of subgrid-scale vertical momentum fluxes,

$$(\frac{\partial \vec{v}}{\partial t})_p = \frac{1}{\rho}\frac{\partial \vec{\tau}}{\partial z}, \qquad \vec{\tau} = -\sum_{j=1}^{n} \rho (\overline{\vec{v'} w'})_j \qquad (2)$$

where the three-dimensional vector $\vec{\tau}(x, y, z)$ is the sum of momentum fluxes due to n different physical processes, denoted here by the index j, ρ is the air density, w is the vertical velocity, an overline denotes gridbox average and a prime $'$ subgrid-scale deviation.

A classical parametrized process is the turbulence over a rough surface. Here, the properties of the surface (aerodynamic roughness) and the flow (thermal stratification, velocity) are accounted for, usually separately for the surface (constant flux) layer between the surface and the lowest model level, and for the layers higher in the planetary boundary layer (PBL) and free atmosphere. Turbulence parametrizations relate the subgrid-scale momentum fluxes to the vertical gradients of the resolved wind components.

In addition, parametrizations of the momentum fluxes due to several other processes including the effects of unresolved small scale orography ("orographic stress"), wave drag due to the breaking orographic or non-orographic buoyancy (gravity) waves, drag due to blocking of the low level flow by mesoscale mountains or effects of local circulations like sea-breeze have been developed.

The concept of effective or orographic roughness length was developed by Fiedler and Panofsky (1972) and Mason (1985). Experimental and theoretical results of Grant and Mason (1990), Wood and Mason (1993), among others, supported the idea that over small scale hills, the area-averaged velocity profile varies logarithmically with height in a similar way as

in the small-scale turbulence. Later, the orographic roughness length has been used in the NWP models as a convenient tuning parameter, even to represent processes of larger scale than it was developed for, see e.g. the model comparison study by Georgelin et al. (2000). An alternative parametrization of the small scale orography effects was proposed by Wood et al. (2001) and Brown and Wood (2001), see also Wilson (2003). Here, a three-dimensional momentum sink is formulated and allowed to influence directly the momentum equations of a NWP model. A practical application of this method to the ECMWF model was suggested by Beljaars et al. (2004).

The need to parametrize the wave drag in NWP models was understood already by Lilly (1972) and applied first by Boer et al. (1984) and Palmer et al. (1986). The first generation parametrizations were based on linear two-dimensional theory of mountain waves developed since 1930'ies (for a review see Smith (1979)). More recent formulations, e.g. Lott and Miller (1997); Gregory et al. (1998); Scinocca and McFarlane (2000) aim at handling also the nonlinear processes of wave generation, breaking and reflection. The blocked-flow drag parametrization by Lott and Miller (1997) uses the approach of an early laboratory study by Hunt and Snyder (1980) and also takes into account directional and asymmetry properties of the unresolved terrain (Baines and Palmer (1990), see also Baines (1998)). A newly formulated mesoscale orography parametrization scheme for the UKMO model (Webster et al., 2003) represents the blocked flow and wave drag by an empirical fit to the numerical simulation results of Olafsson and Bougeault (1997), where also friction and rotation effects were accounted for. An advanced orographic drag parametrization scheme was suggested by Kim and Doyle (2005). It enhances the parametrization of Kim and Arakawa (1995) to take into account the orographic anisotropy and flow blocking. Recent studies by Nappo et al. (2004) and Smith et al. (2005) are devoted to the parametrization of wave stress in the planetary boundary layer.

Each of the different parametrization schemes has been developed based on the knowledge about a particular physical process. However, for historical reasons, new parametrizations have been developed from and combined with the existing ones. Thus, the effective roughness length aimed at parametrization of the unresolved orography effects is combined with the aerodynamic roughness parameter ("vegetation roughness") derived from the land cover characteristics such as vegetation. The parametrized drag due to the flow blocking is formulated as a modification of the wave drag vector. On the other hand, a unified approach to handle wave and turbulent drag due to different scales of orography is still lacking.

Although all the parametrized processes are subgrid-scale relative to a NWP model of a given resolution, the orography scales involved in the different subgrid-scale processes are different. In the parametrization scheme of mesoscale orography effects developed by Scinocca and McFarlane (2000) special care was taken to separate the orography scales treated by the parametrization and resolved by the model. A similar approach is used in derivation of the orography-related parameters for HIRLAM (Rontu et al., 2002) and for the recent version of UKMO model (Webster et al., 2003). A spectral approach is applied in the new parametrization scheme of small-scale orography effects for the ECMWF model (Beljaars et al., 2004).

The purpose of a numerical weather prediction model is to simulate the state of the atmosphere as a whole, including all possible interactions between the processes described by the separate blocks of the model. However, the relations, interactions and scales relevant for the different processes are not always understood and handled systematically. As noted by Kim and Doyle (2005), the distinction among various drag mechanisms near the surface has been rather vague in the literature. Experiments with the parametrization scheme for mesoscale orography effects of the Météo France ARPEGE model (Geleyn et al., 1994), also adapted for HIRLAM, showed that the turbulence and mesoscale orography parametrization schemes are strongly coupled and compensate each other in model simulations (Rontu et al., 2002). In a global model, similar behaviour was revealed by Kim and Hogan (2004).

The aim of the present study is to analyse systematically the influence of the orography-related parametrizations of momentum fluxes on the simulated low level wind and understand the mutual interactions of the parametrized processes. A limited-area atmospheric research and NWP model HIRLAM (Undén et al., 2002) is used as the basic tool and reference model of the study. New parametrization schemes for the meso-scale and smallest-scale orography effects are introduced into HIRLAM. The derivation of orography-related variables of HIRLAM based on digital elevation data is renewed. We will concentrate on lower troposphere momentum fluxes in a synoptic scale version of the model.

The rest of the paper is organised as follows. Section 2 describes the parametrization schemes modified and used in this study. Section 3 presents the derivation of orography-related parameters. Description of the numerical experiments, their results and discussion follow in Sections 4 and 5. Conclusions and outlook finish the study in Section 6.

2 Parametrization schemes

Table 1 lists the parametrization schemes applied and developed in this study. The "reference" refers to the present HIRLAM and "modified" to the suggested parametrizations. A description of the modified schemes is given below. For convenience, a short summary of the relevant reference schemes of HIRLAM is also included. The typical scales of the underlying orography related to the schemes are shown in Table 2 and discussed in more detail in Section 3.

2.1 Turbulent fluxes over flat surface

Momentum flux over a (flat) rough surface is parametrized in HIRLAM in a conventional way (Undén et al., 2002). In the surface layer between the lowest model level and the surface it is defined by the lowest level wind and a drag coefficient:

$$\vec{\tau}_{ts} = -\rho_s (\overline{\vec{v}\,'w'})_{ts} = \rho_s C_u (\vec{v}_{nlev} - \vec{v}_s)|\vec{v}_{nlev}| \tag{3}$$

where $\vec{v}_s = 0$ is the surface wind and $\vec{v}_{nlev}$ denotes wind vector at the lowest model level. (Note that positive surface stress is associated with downward momentum flux.) The indexes s and t refer to surface and turbulence, respectively. The functions used for computation of the aerodynamic resistance in the surface layer are based on Louis (1979) and Louis et al. (1982). The drag coefficient C_u depends on surface roughness, stability and wind shear (Undén et al., 2002). In the reference HIRLAM the momentum roughness consists of both vegetation ($z_{o,veg}$) and orographic ($z_{o,oro}$) components (see Sec. 2.2). In the present modified experiments, only vegetation roughness ($z_{o,veg}$) is used for calculation of the turbulent momentum fluxes. The resulting turbulent stress vector $\vec{\tau}_{ts}$ is turned clockwise (in the Northern Hemisphere) with respect to the surface layer wind $\vec{v}_{nlev}$ in the (stable) boundary layer (Nielsen and Sass, 2004).

The surface turbulent momentum flux given by Eq. (3) defines lower boundary conditions for a $TKE - l$ turbulence scheme based on Cuxart et al. (2000), which parametrizes the turbulent fluxes above the surface layer using the classical eddy diffusivity formula:

$$\vec{\tau}_t = -K \frac{\partial \vec{v}}{\partial z} \tag{4}$$

The coefficient K is computed based on the turbulent kinetic energy TKE and a diagnostic length scale l (Lenderlink and Holtslag, 2004). TKE values are obtained by solving a prognostic equation, for details see Undén et al. (2002).

2.2   *Drag due to unresolved small-scale orography*

In the reference HIRLAM, an orographic roughness length $z_{o,oro}$ is calculated based on the subgrid-scale orography variance and the number of peaks within a grid square (Undén et al., 2002). Empirical scaling parameters are used to enhance the value of this parameter over steep orography (Rontu et al., 2002)[1]. With this approach, all obstacles with a scale smaller than the size of the model's grid-square contribute to the orographic roughness. For the calculation of the surface layer momentum fluxes, $z_{o,oro}$ is combined with the vegetation roughness $z_{o,veg}$ derived from the properties of land cover.

In the present study, a parametrization of small-scale orography (SSO) effects based on Wood et al. (2001) and Brown and Wood (2001), see also Wilson (2003), is implemented in HIRLAM and used instead of the orographic roughness. Here, the orographic stress $\vec{\tau}_o$ due to the small scale orographic features is estimated by the expression

$$\vec{\tau}_o(z) = C_o \frac{\vec{\tau}_{ts}}{\rho_s} s_t^2 \rho(z) e^{-z/l_o} = \vec{\tau}_{os} f(z) \tag{5}$$

where C_o is an orographic drag coefficient, s_t denotes the mean maximum small-scale slope (tangent) over the grid-square, l_o is a decay scale in vertical and z is the height above surface. According to Eq. (5), the surface orographic stress $\vec{\tau}_{os} = C_o \frac{\vec{\tau}_{ts}}{\rho_s} s_t^2$ is parallel to the turbulent stress $\vec{\tau}_{ts}$, which is determined by the wind and stability in model's surface layer (see Sec. 2.1). The vertical decay of the orographic stress is determined by a simple exponential function.

In Eq. (5) several simplifications to the formulae proposed by Wood et al. (2001) were made. The direction differences of slopes and the effects of anisotropy inside the grid-square are ignored, because only the smallest-scale orography (presumably isotropic) features are allowed to influence. The parameter C_o was given a constant value (C_o=2000) instead of taking account its possible dependency on wind shear etc. The value of l_o was set equal to twice the smallest-scale orography standard deviation σ_t in a grid square. Derivation of the variables s_t and σ_t from digital elevation data is discussed in Sec. 3.2.

The suggested formulation differs from that by Beljaars et al. (2004), where a spectral approach to the description of subgrid-scale orography height is applied. With consequent simplifications, the authors end up in an approximation for the tendency of the horizontal wind $\vec{v}(x, y, z)$ (their Eq. (16) rewritten in a form analogous to Eqs. (2) and (5)):

---

[1] Values of the empirical scaling parameters a and B are in the current HIRLAM reference system $a = 0.3430$ and $B = 1.1317$.

$$(\frac{\partial \vec{v}(z)}{\partial t})_o = C_1 |\vec{v}(z)| \vec{v}(z) \sigma_{flt}^2 f_1(z), \tag{6}$$

where C_1 is an orographic drag coefficient; $f_1(z)$ is an empirical function of height derived from the analysis of the spectral properties of small-scale orography; σ_{flt}^2 is a filtered variance of orography height (representing horizontal scales between 5 and 20 km, close to σ_m defined below in Sec. 3.3). Here, the wind tendency at any level depends on the wind at the same level.

2.3 Mesoscale orography effects

A parametrization scheme for mesoscale orography (MSO) effects, developed for the Météo France ARPEGE model, is being implemented into the reference HIRLAM system. The scheme handles vertically propagating buoyancy (gravity) waves and blocking of the low level flow due to mesoscale mountain systems. A short summary is given here, for details see Rontu et al. (2002).

The wave drag is estimated by a formula based on the linear two-dimensional theory,

$$\vec{\tau}_{ws} = K_g \cdot \rho_s \cdot N_s \cdot \vec{v}_{fs} \cdot h_m^2, \tag{7}$$

where the index s refers to mean near-surface values, K_g is a tuning parameter depending on the model resolution (here $K_g = 3.5 \cdot 10^{-06} m^{-1}$), N is the buoyancy (Brunt-Väisalä) frequency, $N^2 = \frac{g}{\theta} \frac{\partial \theta}{\partial z}$, h_m is the subgrid-scale mountain height based on the standard deviation of mesoscale orography and $\vec{v}_{fs}$ is a (fictive) surface wind representing the layer between surface and h_m and parallel to the stress vector $\vec{\tau}_{ws}$.

As long as there is no wave dissipation, the wave momentum flux is constant with height. The momentum sink is realized when the waves break. The parametrization of wave breaking processes follows Lindzen's saturation theory (Lindzen, 1981). In addition, (nonlinear) wave reflection from a breaking level is taken into account. Wave breaking and reflection modify the surface value $\vec{\tau}_{ws}$ and the profile of the wave drag $\vec{\tau}_w(z)$.

Low level flow blocking is assumed if a non-dimensional mountain height G (also called inverse Froude number based on mountain height, see Baines (1998) for clarification of the concepts) depending on stability, mountain height and upstream wind exceeds a critical value. G is defined conveniently as

$$G = N_s \frac{h_m}{U_p} \tag{8}$$

where U_p is the velocity of the upstream wind component perpendicular to the ridge below

h_m. The blocked flow stress $\vec{\tau}_m$ at each (low troposphere) model level is calculated according to Lott and Miller (1997). Finally, it is combined with the wave drag vector $\vec{\tau}_w$.

3   Derivation of orography-related parameters from digital elevation data

The basic variables needed by the parametrization schemes and used for definition of the average terrain height of HIRLAM grid-squares are derived from a digital elevation data set. The reference HIRLAM system uses the GTOPO 30 arc second data (GTOPO30, USGS (1998)) in its original latitude-longitude representation.

In the present study, calculation of the orography-related parameters is renewed and based on the 1 × 1 km resolution Hydro1K elevation derivative database (USGS, 2003). These data are derived from the GTOPO30 data but represented in an equal area azimuthal Lambert projection. Because of the area-conserving properties of this projection, the data set is well suited for further use in the rotated latitude-longitude coordinate system of HIRLAM (Undén et al., 2002). The Hydro1K data, prepared especially for the hydrological use, cover the whole globe excluding Greenland and Antarktis.

Only the terrain elevation of Hydro1K data is used here. From it, the variables listed in Table 2 are calculated for each HIRLAM grid-square of a given resolution. The averages are related to the orography scales indicated in the rightmost column of the table. The choice of 3 km for the limit between small-scale (turbulent) and mesoscale (wave-related) processes is somewhat arbitrary - in reality features of the flow such as stability and flow velocity should influence the definition. The limiting scale between parametrized mesoscale processes and those explicitly resolved by the model's dynamics is chosen to be two grid-lengths (2Δx). Vegetation roughness (whose values in the reference HIRLAM are derived from USGS (1997)) is included into Table 2 for completeness sake.

3.1   Mean elevation

Mean elevation ($H_{2\Delta x}$) is used for calculation of the surface pressure, on which the vertical hybrid coordinate of HIRLAM is based. In the present study it is calculated through double smoothing over a HIRLAM grid-square. First, at each point in the 1 km-resolution Lambert grid, nine-point averages (h_9) of the source Hydro1K elevation (h) data are calculated. These averages now represent an area of 3 × 3 km. They are further averaged, in the rotated HIRLAM coordinate system, over 2Δx-resolution squares centred at the middle of

HIRLAM grid-squares. The rationale behind these operations is to avoid artificial small- and mesoscale features which could be sources of numerical noise for the model integrations. As shown e.g. by Davies and Brown (2001), atmospheric models are not able to explicitly represent underlying orography features smaller than about 4-6 gridlengths.

Smoothing is often achieved through scale-dependent filtering of the mean elevation data. The reference HIRLAM system uses a Raymond filter (Raymond, 1988) for this purpose. Comparison of the reference HIRLAM mean elevation with the one calculated in this study did not reveal significant differences, so the new one is used in all experiments reported in Sec. 4.

3.2   Small-scale orography

The basic parameters for the new orographic turbulence parametrization are the small-scale slope s_t and standard deviation σ_t (see Eq. (5) and related definitions). These parameters are calculated based on the difference between the original (h) and mean (h_9) elevation values. The deviation at the point i,

$$h'_i = h_i - h_{9i} \tag{9}$$

contains only the smallest-scale features. A maximum slope s_{max} is calculated at each Hydro1K point using the difference of h'_i between the point i and its eight neighbours. The maximum slope values are averaged over each HIRLAM grid-square to get the averaged maximum slope s_t. Also the small-scale variance σ_t over a HIRLAM grid-square is derived from the h'_i values.

Distribution of the reference HIRLAM orographic roughness and the new s_t and σ_t in two different resolutions over Iceland is illustrated in Fig. 1. Maximum values and area averages of the main orographic parameters over Iceland are shown in Table 3. General features of the small-scale parameters are somewhat similar. As expected, the new small-scale variables s_t and σ_t are only mildly scale-dependent, as the smallest scale variations should not be sensitive to grid-size. Scale-dependence may only arise because the averages are taken over grid-squares covering areas of different surface types. In addition, the influence of the maximum slopes found in a grid-square is distributed smoothly over larger areas when the resolution grows coarser. Note also the differences along the coastline where the influence of the coarse resolution land-area grid-squares is shows up farther over the sea. The orographic

roughness $z_{o,oro}$ used by the reference HIRLAM system is more sensitive to the change of resolution as it includes all subgrid scales.

3.3   Mesoscale orography

Mesoscale orography variables should represent the orography scales between those resolved by the model dynamics and those included in the parametrization of the smallest-scale orography effects. Here, their values are derived from the difference of the averaged values $h_9 - H_{2\Delta x}$. They are calculated for each grid-point over a square of $2\Delta x \times 2\Delta x$. After the averaging operations, no further filtering of the MSO variables is applied.

The basic variable for the ARPEGE-HIRLAM mesoscale orography (MSO) parametrization scheme is the standard deviation of mesoscale orography σ_m (Fig. 1, Table 3). As expected, its values depend clearly on the model's resolution. The two other MSO parameters are the anisotropy α and the angle θ between model's x-axis and the principal axis (direction of maximum gradient) of the mesoscale orography. All three variables are calculated according to the formulae explained in Rontu et al. (2002) but using the differences $h_9 - H_{2\Delta x}$ instead of the filtered source elevation data.

4   Description of the model experiments

4.1   Definition of the experiments

To test the proposed modifications, a series of one-month simulations in January, 2000 was run using the newest available HIRLAM version (essentially equal to 6.3.5). The two nested experiment domains with horizontal resolutions of 33 km and 11 km are shown in Fig. 2. A model configuration with 40 levels in vertical between the surface and the isobaric level 10 hPa was used. Full data-assimilation with an interval of 6 hours was performed in all experiments. Long forecasts with a length till +48 hours were started once a day at 00 UTC. Lateral boundary values were interpolated from archived HIRLAM analyses with a horizontal resolution of 33 km.

During January 2000 a north-westerly flow over Northern Atlantic towards Scandinavia was prevailing. Over Iceland, the mean flow was westerly, with an orographic anticyclone forming over the high elevation glacier Vatnajökull. During 25-27 January there was significant wave activity over Scandinavian mountains, indicated also by the observed stratospheric wave clouds (Dörnbrack et al., 2002).

The main numerical experiments are summarized in Table 4. MSO refers to the mesoscale (Sec. 2.3) and SSO to small-scale (Sec. 2.2) orography parametrizations. ECMWF SSO parametrizations are based on Eq. (6), where σ_m from the present 11 km resolution experiments is taken to represent σ_{flt} and coefficients are taken from Beljaars et al. (2004), while HIRLAM SSO parametrizations use Eqs. (2) and (5). The experiments are referred to as R33 or O11 etc., to indicate both the experiment name and horizontal resolution. Note that the new mean orography (see Sec. 3.1) was used in all experiments.

4.2 Diagnostic variables and tools

Averaging Eq. (1) over long enough period of time allows to estimate the response of model dynamics to the forcing due to the physical processes.[2] The three-dimensional wind tendency (Eqs. (2), (6)) due to a physical process can be integrated vertically to obtain the corresponding surface stress, assuming that there are no vertical momentum fluxes at the top of the model atmosphere. Diagnostics collected at each time step of a HIRLAM experiment include accumulated tendencies of model variables (such as wind components or derived from these resolved scale kinetic energy) plus independently accumulated surface fluxes. These allow to understand the role of different parametrized processes and the response of model dynamics.

The resolved-scale kinetic energy can be used for the analysis of the results of the numerical experiments. Its true sources and sinks represent the work done by frictional forces, i.e. the parametrized turbulence, mesoscale and small scale orography effects. It can be estimated based on the values of wind components and their accumulated tendencies:

$$(\frac{\partial k}{\partial t})_j = \frac{\partial \frac{\rho}{2}(u^2 + v^2)}{\partial t} \approx \rho u(\frac{\partial u}{\partial t})_j + \rho v(\frac{\partial v}{\partial t})_j, \tag{10}$$

where $k = \frac{\rho}{2}(u^2 + v^2)$ denotes the (diagnostic) resolved-scale kinetic energy and the index j denotes any of the different processes so that $j = d, t, o, m$ refer to dynamics, turbulence, SSO or MSO parametrizations, respectively. The total tendency, due to the model dynamics and all parametrizations, is obtained from the difference of two model states. Averaged over long enough time it is close to zero so that the dynamical and parametrized tendencies balance each other.

Analysis of the results is performed over the common area of the experiments (see Fig. 2).

---

[2] Note that the "dynamical tendency" does not mainly refer to the resolved-scale mountain waves, although their influence is included in it.

For the comparison, results of the coarse resolution experiments are interpolated to the fine resolution grid. Special attention is paid to the behaviour of the parametrizations over the complex orography of Iceland. In addition, the standard station verification provides bias and root-mean-square errors of the forecasts against observations.

5   Results and discussion

5.1   Surface stress

A west-east cross-section over Southern Iceland (along the line shown in Fig. 1) illustrates a typical behaviour of surface momentum fluxes or surface stress components due to turbulence, small- and mesoscale orography (Fig. 3). Results of the experiments O11/O33 and B11/B33 are shown. Several features can be noted: 1) the effect of the MSO parametrizations decreases dramatically with improving resolution, 2) turbulent and SSO stress increase slightly with increasing resolution, 3) the role of orographic turbulence is significantly larger in the experiments 'B' compared with the experiments 'O'. The total surface drag, i.e. the sum of $|\vec{\tau}_{ts}|$, $|\vec{\tau}_{os}|$ and $|\vec{\tau}_{ms}|$, is shown in Fig. 4. It can be seen that the total drag increases from the experiments 'R' and 'O' to 'B'. Improvement of the resolution leads to a decrease of the parametrized drag in the experiments 'O' and 'B' but not in the experiments 'R'.

The different behaviour of the total surface stress in the experiments is illustrated by Fig. 5 for the whole Iceland in the case of 33 km resolution. The experiment B33 produces clearly larger stress than R33 and O33, the difference increasing with the increasing total stress values. The difference is less pronounced over the whole European experiment domain and practically nonexistent over flat land areas (not shown). The differences are also smaller in the 11 km experiments.

Finally, Table 5 summarizes the comparison of averaged over whole Iceland parametrized surface stress due to the different processess and systematic differences between experiments of different resolutions. The numbers confirm the conclusions based on Figs. 3-5. Interactions between the parametrization schemes are further discussed in the next section.

5.2   Kinetic energy budget

Vertical profiles of the area-averaged kinetic energy tendencies are compared in Figs. 6 and 7. In the reference HIRLAM, turbulence - based on the effective roughness - is the only parametrized process responsible for the subgrid-scale change of the resolved-scale kinetic

energy (experiment R33 in Fig. 6, upper panel). Its influence and the response of model's dynamics balance each other in the whole planetary boundary layer (PBL), in this case till the model level 30, i.e. approximately to the height of 1.5 km. In the experiment O33 the effects of MSO and SSO parametrizations are smaller than that of the parametrized turbulence and seen in a shallower layer (Fig. 6, upper panel). As soon as these parametrizations are included, compensation between the schemes shows up (see the difference in Fig. 6, lower left), as noted earlier by Rontu et al. (2002). The dynamic response due to the total stress divergence changes only a little.

Comparison of the different resolution experiments O11 and O33 (Fig. 6, lower right) shows, with improving resolution, a decrease of the MSO effect and a corresponding increase of the turbulence and SSO effects on kinetic energy. In this case the dynamic response also changes, i.e when the resolution grows higher, the predicted kinetic energy tendency due to the parametrized processes tends to increase at the lowest levels and decrease in the upper part of the PBL, i.e. the effects concentrate on a shallower layer.

Experiments 'B' behave differently from the experiments 'O' both in the high and the low resolution cases (Fig. 7, upper panel for the 33 km resolution, comparison between O11 and B11 not shown). In B11 and B33 the small-scale orography effects dominate the mesoscale effects and tend to retard the flow in a deep layer. Close to the surface the compensating effect of the non-orographic turbulence increases in 'B' (even creating resolved-scale kinetic energy!) compared to 'O'. Compared to 'O' (Fig. 7, lower left) and 'R' (not shown), the experiments 'B' seem to create the strongest dynamic response (retardation) in the upper part of the PBL. The difference between experiments B11 and B33 is mainly due to the decrease of the MSO effect as in the case of the experiment O11 compared to O33.

MSO, SSO and turbulence parametrization schemes are coupled with each other mainly through the low level wind velocity (see Sec. 5.3 for discussion of the low level wind), which influences all the surface stress components. The surface layer stability is expected to play a minor role. In the HIRLAM system, each of the parametrization schemes independently creates a wind tendency $\frac{\partial \vec{v}}{\partial t}$ using wind vector values at the previous time step. Before starting the next time step, these contributions are summed. They are then added to the tendency due to the model dynamics, and the values of the wind components updated accordingly.

In the model, a (non-orographic) turbulence parametrization scheme tends to smooth subgrid-scale vertical gradients independently of their origin or scale. The orography-related parametrizations and model dynamics, each within their own horizontal and vertical scales,

may create such gradients. This might offer a possible mechanism of compensation between the schemes, shown in Figs. 6 and 7.

5.3   Surface pressure and low level winds

In HIRLAM, a long-lasting feature seen in comparisons of the predicted with observed ten-metre level wind (V_{10m}), has been a systematic overestimation of wind speed by 0.5 - 1 ms^{-1}. In the present study, standard station verification (bias and root-mean-square error) against synoptic observations over European or Scandinavian land stations did not reveal significant differences between the experiments O33 and R33 during January 2000 (not shown). In the experiment B33, the typical for the reference HIRLAM positive bias of V_{10m} is slightly improved but a small positive mean sea level pressure (pmsl) bias of about 0.2 hPa appears. Small changes of the two-metre temperature and humidity bias also appear. Verification of all 11 km experiments over Scandinavia shows negligible differences. Thus, the possible effects of orography-related parametrizations seem to be mostly local. In the following, verification results over Iceland are analysed more closely.

Here, instead of the familiar positive bias of V_{10m}, there is a negative one, of about -1 ... -1.5 ms^{-1} (depending on the forecast length) in 'R' and 'O', and about -2 ms^{-1} in 'B', with a corresponding positive pmsl bias - the smallest in 'R' - of the order of 0.2 - 0.8 hPa (comparison not shown). Thus, the near-surface wind seems to be retarded too much in all experiments, and the unmodified reference HIRLAM gives the best results. In all experiments the rms error is larger (5-6 ms^{-1}) over Iceland than over Scandinavian or European area (3-4 ms^{-1}). The behaviour of the 11 km and the 33 km experiments is similar, with the exception of somewhat better pmsl scores in the fine resolution.

Fig. 8 shows the difference between observed and predicted pmsl and V_{10m} given by the +48h forecasts of the experiments R33, O33 and B33 over the Icelandic synoptic stations (ca. 10 stations available for the operational data assimilation each night[3]), classified according to the observed wind velocity. It can be seen that over Iceland, the negative wind bias is due to underprediction of the moderate and strong winds. The error is partly compensated by overprediction of weak winds, especially in the case of the reference experiment R33. The

---

[3] The possible problems of representativeness and actual observation levels etc. are not discussed in this study but the measurements are taken to represent the true V_{10m} values.

increased drag of B33 leads to retardation of all winds and consequently, to worse overall verification scores. In O33, retardation of the strong winds is the smallest.

Thus, when weak winds dominate (over the whole Scandinavian/European integration area, not shown), the results show a positive bias. In Iceland, moderate and strong winds dominate, leading to a negative wind bias and a positive pressure bias. To correct the systematic error of the low level wind prediction, weak winds should be retarded and strong winds accelerated in both cases. The proposed orography-related parametrizations do not solve this problem, although the experiments 'O' seem to take a step in right direction. This is shown in Fig. 9, where the distribution of the lowest model level wind (level 40 centered at the height of 32 m) over Iceland is compared between the experiments O33, B33 and R33. It is seen that the weak winds are weaker and strong winds stronger in O33 compared to R33, while all winds are weaker in B33 compared to R33 and O33. However, the results of R33 and O33 remain quite close to each other, indicating that the improvement obtained by modifying the orography-related surface drag is still insufficient.

6   Conclusions

Three different subgrid-scale processes contribute to the momentum budget of HIRLAM in the planetary boundary layer (PBL): turbulent diffusion, orographic turbulence related to the smallest-scale orography (SSO) and wave-related effects (in fact, blocking of the low level flow by mesoscale mountains) due to the mesoscale orography (MSO). In the reference model, orographic roughness ($z_{o,oro}$) is used to parametrize all orography-related processes. In this study $z_{o,oro}$ was replaced by new parametrizations for small-scale (SSO) and mesoscale (MSO) orography effects. For the SSO parametrizations, two different approaches were tried: the HIRLAM formulation (Eq. 5) and the ECMWF formulation (Eq. 6). Needed orographic parameters were derived from fine resolution (Δx=1 km) digital elevation data.

In order to compare the parametrizations, numerical experiments over Europe were run in January 2000. Coarse (with a horizontal grid-length of 33 km) and fine resolution (11 km) results were compared. A simple verification of forecasts against (SYNOP) observations turned out to be too smoothing to reveal and understand the differences between the experiments. Momentum fluxes, kinetic energy budget and detailed analysis of observation-forecast differences were thus used. Particular attention was paid to the results over the complex orography of Iceland.

Analysis of the surface momentum fluxes showed, as expected, that the influence of the MSO parametrizations decreases when the resolution improves. The surface drag due to the ECMWF-style SSO parametrizations was found to be significantly larger than that given by the reference HIRLAM or the HIRLAM-style SSO parametrizations. It also influenced in deeper layer, dominating over the mesoscale effects even in the coarse resolution experiments. Analysis of the kinetic energy budgets showed that the different parametrizations tend to compensate each other. Although the MSO and SSO parametrizations feel the details of different subgrid scales of the underlying orography, the turbulence parametrizations and model dynamics are only able to separate processess larger or smaller than the grid scale, thus possibly smoothing all gradients irrespectively to their origin.

Analysis of forecast-observation differences over different areas showed that the orography-related parametrizations influence in quite local scale. Over flat areas, only minor differences between the experiments were seen. Both the reference HIRLAM and the modified versions tend to overestimate weak and underestimate strong winds in coarse and fine resolution experiments. A model version with the new HIRLAM-style SSO parametrizations combined with new MSO parametrizations was able to correct this distribution slightly, while the use of the ECMWF-style SSO parametrizations led to a retardation of all winds.

In the future, more extensive model comparisons would be needed in order to fine-tune the new parametrizations. Dependencies between the orography-related parametrizations and the TKE-based turbulence scheme might be analysed further in order to improve the overall result. The behaviour and need of the parametrizations for subgrid-scale orography effects in the fine-scale models (with a kilometre-scale horizontal gridlength and non-hydrostatic dynamics) requires further studies. In this case, even the one-kilometre resolution elevation data would be insufficiently detailed for derivation of the needed subgrid-scale orographic variables. The diagnostic tools developed and applied in the present study are believed to be useful also in the analysis of the future experiments.

REFERENCES

Baines, P., 1998: *Topographic effects in stratified flows*. Cambridge University Press, 482 pp.

Baines, P., and T. Palmer, 1990: Rationale for a new physically based parametrization of sub-grid scale orographic effects. ECMWF Tech. Memo 169. ECMWF, Shinfield Park, Reading, Berkshire, U.K.

Beljaars, A. C. M., A. R. Brown, and N. Wood, 2004: A new parametrization of turbulent orographic form drag. *Quart. J. Roy. Met. Soc.*, **130**, 1327–1347.

Boer, G. J., N. A. McFarlane, R. Laprise, J. D. Henderson, and J.-P. Blanchet, 1984: The Canadian Climate Centre spectral atmospheric general circulation model. *Atmos. Ocean.*, **22**, 397–429.

Brown, A. R., and N. Wood, 2001: Turbulent form drag on anisotropic three-dimensional orography. *Bound. Lay. Met.*, **101**, 229–241.

Cuxart, J., P. Bougeault, and J. L. Redelsberger, 2000: A turbulence scheme allowing for mesoscale and large-eddy simulations. *Quart. J. Roy. Met. Soc.*, **126**, 1–30.

Davies, L. A., and A. R. Brown, 2001: Assesment of which scales of orography can be credibly resolved in a numerical model. *Quart. J. Roy. Met. Soc.*, **127**, 1225–1236.

Dörnbrack, A., T. Birner, A. Fix, H. Flentje, A. Meister, H. Schmid, E. Browell, and M. J. Mahoney, 2002: Evidence for intertia-gravity waves forming polar stratospheric clouds over Scandinavia. *J. Geoph. Res.*, **107**(D20), 8287, doi:10.1029/2001JD000452.

Fiedler, F., and H. A. Panofsky, 1972: The geostrophic drag coefficient and the "effective" roughness length. *Quart. J. Roy. Met. Soc.*, **98**, 213–220.

Geleyn, J.-F., E. Bazile, P. Bougeault, M. Déqué, V. Ivanovici, and coauthors, 1994: Atmospheric parametrisation schemes in Météo-France's ARPEGE N.W.P. model. Proc. Seminar on Physical Parametrization for Numerical Models. ECMWF, Shinfield Park, Reading, Berkshire, U.K., 385-402.

Georgelin, M., P. Bougeault, T. Black, N. Brzovic, A. Buzzi, and coauthors, 2000: The second COMPARE exercise: A model intercomparison using a case of a typical mesoscale orographic flow, the PYREX IOP3. *Quart. J. Roy. Met. Soc.*, **126**, 991–1029.

Grant, A. L. M., and P. Mason, 1990: Observations of boundary-layer structure over complex terrain. *Quart. J. Roy. Met. Soc.*, **116**, 159–186.

Gregory, D., G. J. Shutts, and J. R. Mitchell, 1998: A new gravity-wave-drag scheme incorporating anisotropic orgraphy and low-level wave breaking: Impact upon the climate of the UK Meteorological Office Unified Model. *Quart. J. Roy. Met. Soc.*, **124**, 463–493.

Hunt, C. R., and W. H. Snyder, 1980: Experiments on stably stratified flow over a model three-dimensional hill. *J. Fluid Mech.*, **96**, 671–704.

Kim, Y.-J., and A. Arakawa, 1995: Improvement of orographic gravity wave parametrization using a mesoscale gravity wave model. *J. Atm. Sci.*, **52**, 1875–1902.

Kim, Y.-J., and J. D. Doyle, 2005: Extension of an orographic drag parametrization scheme to incorporate orographic anisotropy and flow blocking. *Quart. J. Roy. Met. Soc.* in press.

Kim, Y.-J., and T. F. Hogan, 2004: Response of a global atmospheric model to various drag parametrizations. *Tellus*, **56A**, 472–484.

Lenderlink, G., and B. Holtslag, 2004: An updated length scale formulation for turbulent mixing in clear and cloudy boundary layers. *Quart. J. Roy. Met. Soc.*, **130**, 3405–3427.

Lilly, D. K., 1972: Wave momentum flux - a GARP problem. *Bull. Am. Met. Soc.*, **53**, 17–23.

Lindzen, R. S., 1981: Turbulence and stress due to gravity wave and tidal breakdown. *J. Geoph. Res.*, **86**, 9707–9714.

Lott, F., and M. Miller, 1997: A new subgrid-scale orographic drag parametrization: Its formulation and testing. *Quart. J. Roy. Met. Soc.*, **123**, 101–127.

Louis, J., 1979: A parametric model of vertical eddy fluxes in the atmosphere. *Bound. Lay. Met.*, **17**, 187–202.

Louis, J. F., M. Tiedtke, and J.-F. Geleyn, 1982: A short story of the PBL parameterization at ECMWF. Proceedings of the ECMWF Workshop on Planetary Boundary Layer Parameterization, 25-27 November 1981. ECMWF, Shinfield Park, Reading, Berkshire, U.K.

Mason, P. J., 1985: On the parameterization of the orographic drag. Proc. Seminar on Physical parametrization for Numerical Models of the Atmosphere. ECMWF, Shinfield Park, Reading, Berkshire, U.K., 139-165.

Nappo, C. J., H.-Y. Chun, and H.-J. Lee, 2004: A parametrization of wave stress in the planetary boundary layer for use in mesoscale models. *Atm. Env.*, **38**, 2665–2675.

Nielsen, N. W., and B. H. Sass, 2004: Rotation of the surface stress as a tool in parameterization of atmospheric turbulence. *DMI Scientific Report*, **04-07**, Available at http://www.dmi.dk.

Olafsson, H., and P. Bougeault, 1997: The effect of rotation and surface friction on orographic drag. *J. Atm. Sci.*, **54**, 193–210.

Palmer, T. N., G. J. Shutts, and R. Swinbank, 1986: Alleviation of a systematic westerly bias in general circulation and numerical weather prediction models through an orographic gravity-wave drag parametrization. *Quart. J. Roy. Met. Soc.*, **112**, 1001–1039.

Raymond, W. H., 1988: High-order low-pass implicit tangent filters for use in finite area calculations. *Mon. Wea. Rev.*, **116**, 2132–2141.

Rontu, L., K. Sattler, and R. Sigg, 2002: Parametrization of subgrid-scale orography effects in HIRLAM. Technical Report 56, HIRLAM, 46pp. Available at http://hirlam.knmi.nl.

Scinocca, J. F., and N. A. McFarlane, 2000: The parametrization of drag induced by stratified flow over anisotropic orography. *Quart. J. Roy. Met. Soc.*, **126**, 2353–2393.

Smith, R. B., 1979: The influence of mountains on the atmosphere. *Adv. Geoph.*, **21**, 87–230.

Smith, R. B., Q. Jiang, and J. D. Doyle, 2005: A theory of gravity wave absorption by a boundary layer. *J. Atm. Sci.* submitted.

Undén, P., L. Rontu, H. Järvinen, P. Lynch, J. Calvo, and coauthors, 2002: The HIRLAM-5 Scientific documentation, December 2002. Available at http://hirlam.knmi.nl.

USGS, 1997: The Global Land Characteristics Data Base. U.S. Geological Survey, available at http://edcdaac.usgs.gov/glcc/glcc.html.

USGS, 1998: GTOPO30, Global 30 Arc Second Elevation Data Set. U.S. Geological Survey, available at http://edcdaac.usgs.gov/gtopo30/gtopo30.html.

USGS, 2003: Hydro1k elevation derivative database. http://edcdaac.usgs.gov/gtopo30/hydro/readme.html.

Webster, S., A. R. Brown, D. R. Cameron, and P. Jones, 2003: Improvements to the representation of orography in the Met Office Unified Model. *Quart. J. Roy. Met. Soc.*, **129**, 1989–2010.

Wilson, J. D., 2003: Representing drag on unresolved terrain as a distributed momentum sink. *J. Atm. Sci.*, **99**, 1629–1637.

Wood, N., A. R. Brown, and F. E. Hewer, 2001: Parametrizing the effects of orography on the boundary layer: An alternative to effective roughness lengths. *Quart. J. Roy. Met. Soc.*, **127**, 759–777.

Wood, N., and P. J. Mason, 1993: The pressure force induced by neutral, turbulent flow over hills. *Quart. J. Roy. Met. Soc.*, **119**, 1233–1267.

Table 1. Parametrization schemes of subgrid-scale momentum fluxes. See the text for explanations and notation.

drag	related to	momentum sink	reference	modified
$\vec{\tau}_{ts}$	turbulent drag due to surface roughness	surface (2D)	$z_{o,veg}+z_{o,oro}$	$z_{o,veg}$
$\vec{\tau}_o$	drag due to unresolved small-scale orography	internal (3D)	$z_{o,veg}+z_{o,oro}$	SSO parametrization
$\vec{\tau}_m$	blocked flow drag due to mesoscale orography	internal (3D)	-	MSO parametrization
$\vec{\tau}_w$	drag due to breaking buoyancy waves	internal (3D)	-	MSO parametrization
$\vec{\tau}_t$	turbulence (vertical diffusion)	internal (3D)	$TKE-l$	$TKE-l$

Table 2. Orography variables derived from digital elevation data

parameter	definition	horizontal scale of orography
	for resolved dynamics	
$H_{2\Delta x}$	mean height	$> 2\Delta x$
	for MSO parametrizations	
σ_m	standard deviation	3 km - $2\Delta x$
α	anisotropy	3 km - $2\Delta x$
θ	direction angle	3 km - $2\Delta x$
	for SSO parametrizations	
s_t	maximum slope s_{max}	< 3 km
σ_t	standard deviation	< 3 km
	for turbulence parametrizations	
$z_{o,veg}$	vegetation roughness	<< 1 km

Table 3. Orography characteristics over Iceland

parameter	resolution	maximum	mean	unit
$H_{2\Delta x}$	33 km	1357	225	m
	11 km	1665	225	m
σ_m	33 km	531	143	m
	11 km	584	80	m
s_t	33 km	1.5	0.26	deg
	11 km	2.2	0.26	deg
σ_t	33 km	120	17	m
	11 km	90	19	m
$z_{o,oro}$	33 km	6.85	0.51	m
	11 km	6.85	0.26	m

Table 4. Definition of the numerical experiments

experiment	description
R33 and R11	reference HIRLAM
O33 and O11	MSO + SSO parametrizations
B33 and B11	MSO + ECMWF SSO parametrizations

Table 5. Surface stress over Iceland in January 2000: mean and standard deviation over the area. Unit and time averages as in Fig. 3.

experiment	$|\vec{\tau}_{ts}|$	$|\vec{\tau}_{os}|$	$|\vec{\tau}_{ms}|$	total
O11	0.41±0.12	0.05±0.09	0.21±0.30	0.67±0.34
O33	0.35±0.10	0.03±0.03	0.43±0.42	0.82±0.37
O11-O33	0.05±0.11	0.02±0.07	-0.22±0.35	-0.15±0.36
B11	0.26±0.13	0.29±0.27	0.28±0.37	0.83±0.57
B33	0.22±0.09	0.22±0.22	0.56±0.50	1.02±0.58
B11-B33	0.04±0.09	0.04±0.30	-0.27±0.42	-0.19±0.51
R11	0.67±0.35	-	-	0.67±0.35
R33	0.70±0.24	-	-	0.70±0.24
R11-R33	-0.03±0.28	-	-	-0.03±0.28

Figure captions

Fig.1.

Orography parameters over Iceland, from left to right: s_t (degrees, isoline spacing 0.4 deg), σ_t (metres, isoline spacing 20 m, σ_m (metres, isoline spacing 100 m), $z_{o,oro}$ (metres, isoline spacing 0.4 m), with a horizontal grid-size of 11 km (upper row) and 33 km (lower row). Dashed line along rotated latitude 6.8 N shows the line of cross-sections discussed in Sec. 5, dotted lines show selected geographic latitudes and longitudes.

Fig 2.

Integration areas of the 33 km (full area of the map) and 11 km (box outlined by dashed line) experiments. Shown in the figure are isolines of the surface elevation (whole area, isoline spacing 300 m) and mean sea level pressure averaged over January 2000 (small area, given by the 00UTC+48h forecasts of the experiment R33, isoline spacing 5 hPa).

Fig 3.

Surface stress components $|\vec{\tau}_{ts}|$ (solid), $|\vec{\tau}_{os}|$ (dotted) and $|\vec{\tau}_{ms}|$ (dashed) with the resolutions 11 km (circles on the lines) and 33 km (no markers), for the experiments O11 and O33 (a) and for the experiments B11 and B33 (b), averaged over 31 00UTC+48h forecasts along the rotated latitude 6.8 N in Southern Iceland, unit Pa. To retain only significant features, the time-averaged model output fields were spectrally smoothed before drawing the cross section values.

Fig. 4.

Magnitude of the total surface stress $|\vec{\tau}_{ts}|+|\vec{\tau}_{os}|+|\vec{\tau}_{ms}|$ with the resolutions 33 km (left) and 11 km (right), for the experiments 'O' (open circles), 'B' (filled circles) and 'R' (crosses). Note that in the reference HIRLAM ('R') the sum consists only of the turbulent component based on effective roughness. Cross-section, unit, time averages and smoothing as in Fig. 3.

Fig. 5.

Magnitude of the total surface stress of the reference experiment R33 (x-axis, both figures) compared with that of O33 (y-axis, a) and B33 (y-axis, b) over Iceland with the open sea grid-points excluded. Based on accumulated values of 31 00UTC+48h forecasts during January 2000. A least squares line is fitted in the scatterplot, with calculated correlations of 0.81 (R33/O33) and 0.83 (R33/B33). Note that the scales of x- and y-axes are different. Unit as in Fig. 3.

Fig. 6.

Resolved scale kinetic energy tendencies due to the effects of parametrized turbulence (turb, long-dashed), meso-scale orography (mso, dotted) and small-scale orography (sso, long-short-dashed), averaged over the area of Iceland and based on the accumulated tendencies of 31 00UTC+48h forecasts during January 2000. The response of model dynamics, equal in magnitude and opposite in sign to the sum of parametrized processes, is also shown (dyn, solid). Figures from left to right: R33, O33, O11 (upper row), R33-O33, O11-O33 (lower row). Unit kJkg^{-1}day^{-1}. Vertical axis: model level from the bottom (level 40, ca. 32 m) to the middle troposphere (level 20, ca. 5 km). The uppermost 19 model levels are not shown. In this figure, every model layer gets equal weight in spite of the different thicknesses of the layers. Note the different horizontal scales of upper and lower rows.

Fig. 7.

As Fig. 6, but figures from left to right: O33, B33, B11 (upper row), O33-B33, B11-B33 (lower row).

Fig. 8

Systematic difference between predicted and observed (00 UTC+48h forecasts - 00 UTC observations) mean sea level pressure (hPa, upper panel, left y-axis) and ten-metre wind speed (ms^{-1}, lower panel, left y-axis) at the Iceland synoptic stations in January 2000, classified according to observed pressure (hPa, upper panel, x-axis) or wind (ms^{-1}, lower panel, x-axis). Number of observations in each class is shown by shaded bars (right y-axes). The lines with squares show the bias of each class. Lines with circles show the accumulated weighted contribution of the classes to the total bias of 00UTC+48h forecasts, which value is thus shown by the rightmost circle of each line. Experiments from left to right: R33, O33, B33.

Fig. 9.

Magnitude of the lowest model level wind (ms^{-1}) of the experiment O33 (y-axis, a) and B33 (yaxis, b) compared with that of R33 (x-axis, both figures) over Iceland with the open sea grid-points excluded. Based on 31 00UTC+48h forecasts during January 2000. A least squares line is fitted in the scatterplot, with calculated correlations of 0.95 (O33/R33) and 0.92 (B33/R33).
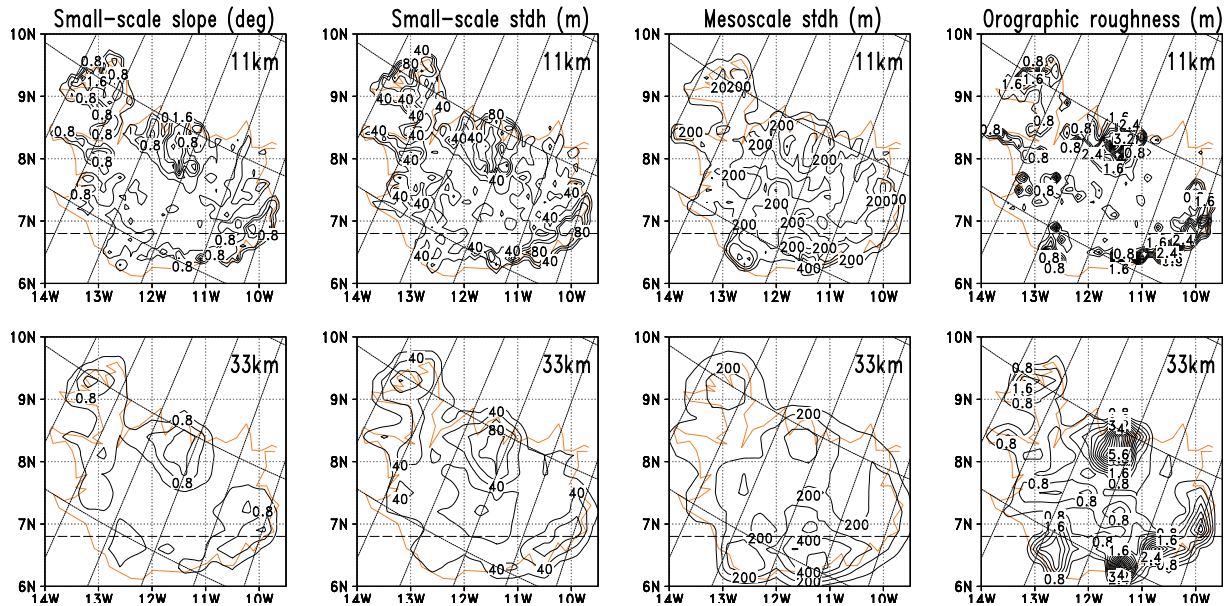
Figure 1. *Orography parameters over Iceland, from left to right: s_t (degrees, isoline spacing 0.4 deg), σ_t (metres, isoline spacing 20 m, σ_m (metres, isoline spacing 100 m), $z_{o,oro}$ (metres, isoline spacing 0.4 m), with a horizontal grid-size of 11 km (upper row) and 33 km (lower row). Dashed line along rotated latitude 6.8 N shows the line of cross-sections discussed in Sec. 5, dotted lines show selected geographic latitudes and longitudes.*
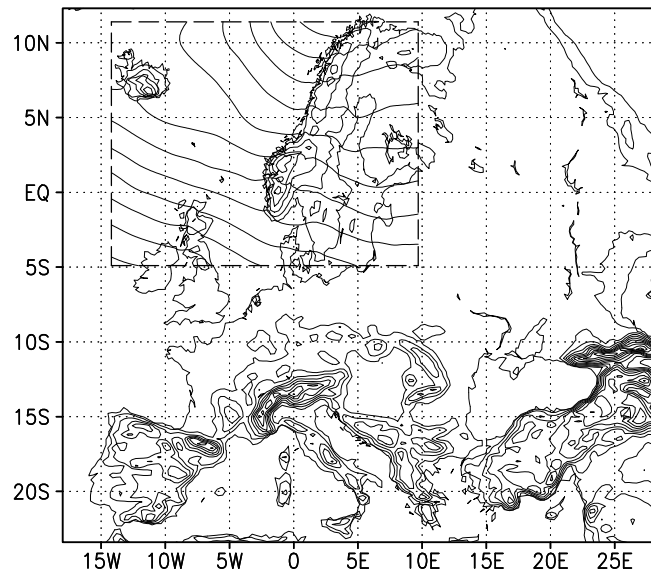

Figure 2. *Integration areas of the 33 km (full area of the map) and 11 km (box outlined by dashed line) experiments. Shown in the figure are isolines of the surface elevation (whole area, isoline spacing 300 m) and mean sea level pressure averaged over January 2000 (small area, given by the 00UTC+48h forecasts of the experiment R33, isoline spacing 5 hPa).*

(a)

(b)
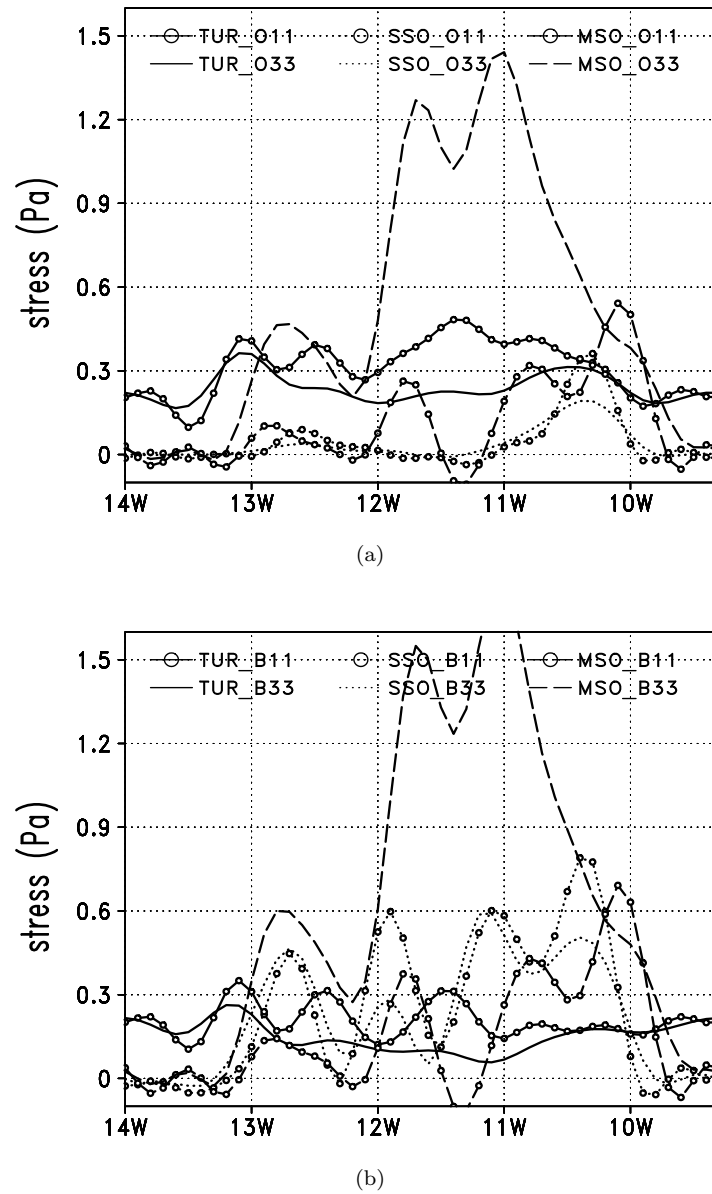
Figure 3. *Surface stress components $|\vec{\tau}_{ts}|$ (TUR, solid), $|\vec{\tau}_{os}|$ (SSO, dotted) and $|\vec{\tau}_{ms}|$ (MSO, dashed) with the resolutions 11 km (circles on the lines) and 33 km (no markers), for the experiments O11 and O33 (a) and for the experiments B11 and B33 (b), averaged over 31 00UTC+48h forecasts along the rotated latitude 6.8 N in Southern Iceland, unit Pa. To retain only significant features, the time-averaged model output fields were spectrally smoothed before drawing the cross section values.*
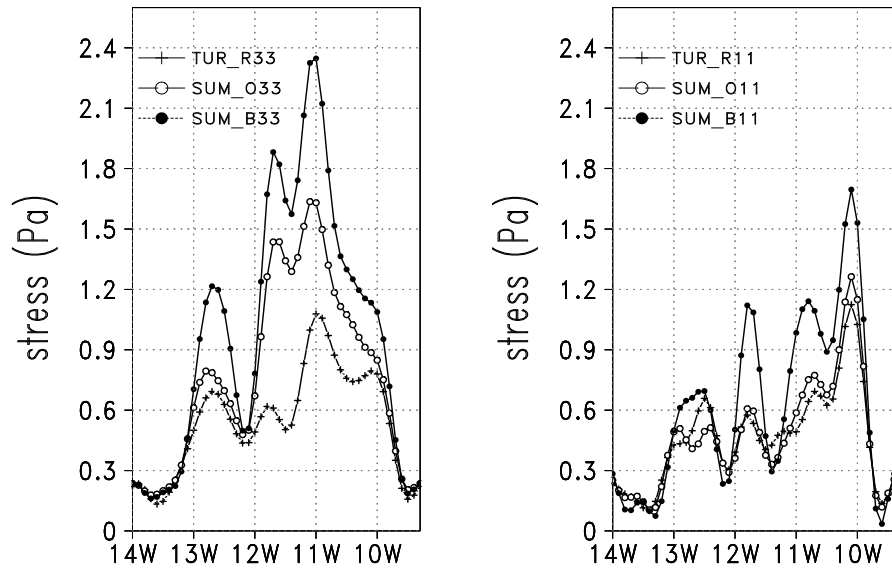
Figure 4. *Magnitude of the total surface stress $|\vec{\tau}_{ts}|+|\vec{\tau}_{os}|+|\vec{\tau}_{ms}|$ with the resolutions 33 km (left) and 11 km (right), for the experiments 'O' (open circles), 'B' (filled circles) and 'R' (crosses). Note that in the reference HIRLAM ('R') the sum consists only of the turbulent component based on effective roughness. Cross-section, unit, time averages and smoothing as in Fig. 3.*
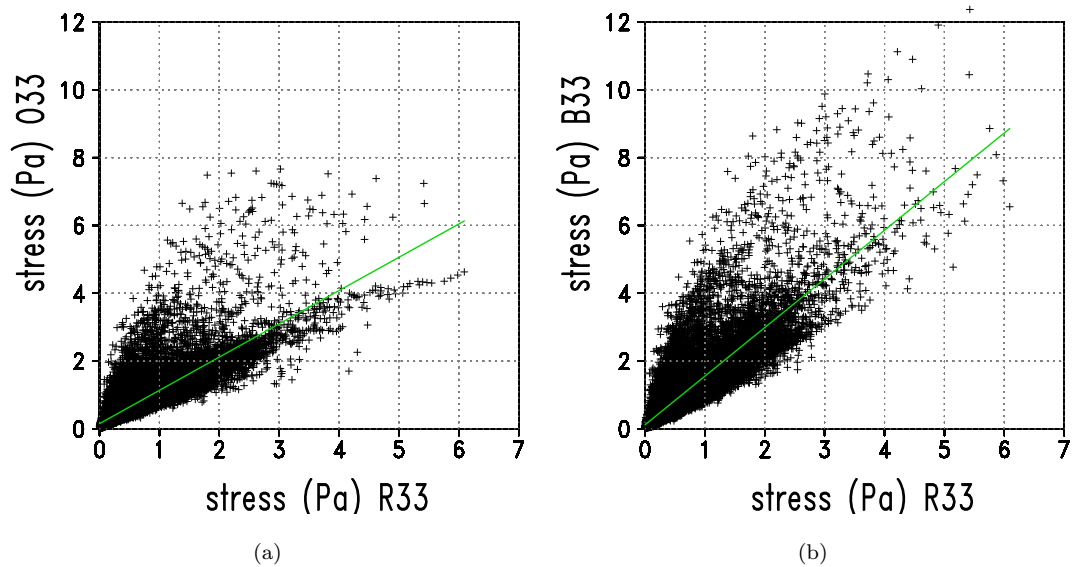

Figure 5. *Magnitude of the total surface stress of the reference experiment R33 (x-axis, both figures) compared with that of O33 (y-axis, a) and B33 (y-axis, b) over Iceland with the open sea grid-points excluded. Based on accumulated values of 31 00UTC+48h forecasts during January 2000. A least squares line is fitted in the scatterplot, with calculated correlations of 0.81 (R33/O33) and 0.83 (R33/B33). Note that the scales of x- and y-axes are different. Unit as in Fig. 3.*
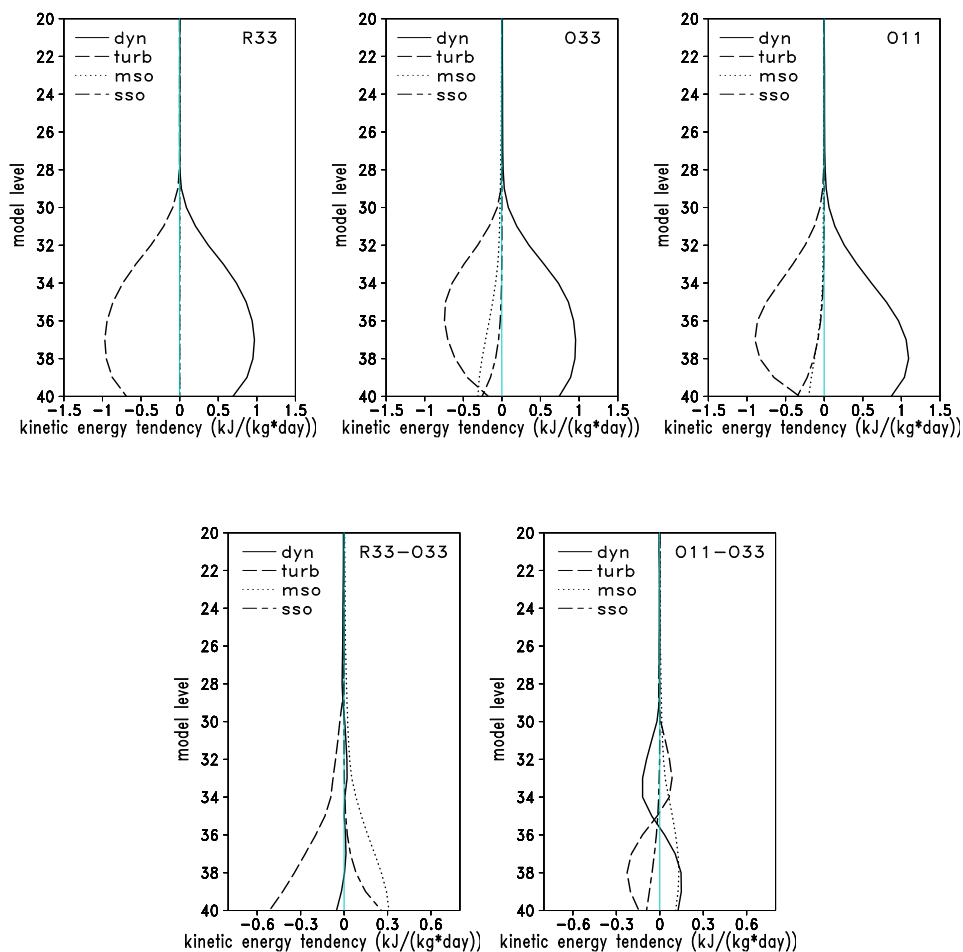
Figure 6. *Resolved scale kinetic energy tendencies due to the effects of parametrized turbulence (turb, long-dashed), meso-scale orography (mso, dotted) and small-scale orography (sso, long-short-dashed), averaged over the area of Iceland and based on the accumulated tendencies of 31 00UTC+48h forecasts during January 2000. The response of model dynamics, equal in magnitude and opposite in sign to the sum of parametrized processes, is also shown (dyn, solid). Figures from left to right: R33, O33, O11 (upper row), R33-O33, O11-O33 (lower row). Unit $kJkg^{-1}day^{-1}$. Vertical axis: model level from the bottom (level 40, ca. 32 m) to the middle troposphere (level 20, ca. 5 km). The uppermost 19 model levels are not shown. In this figure, every model layer gets equal weight in spite of the different thicknesses of the layers. Note the different horizontal scales of upper and lower rows.*
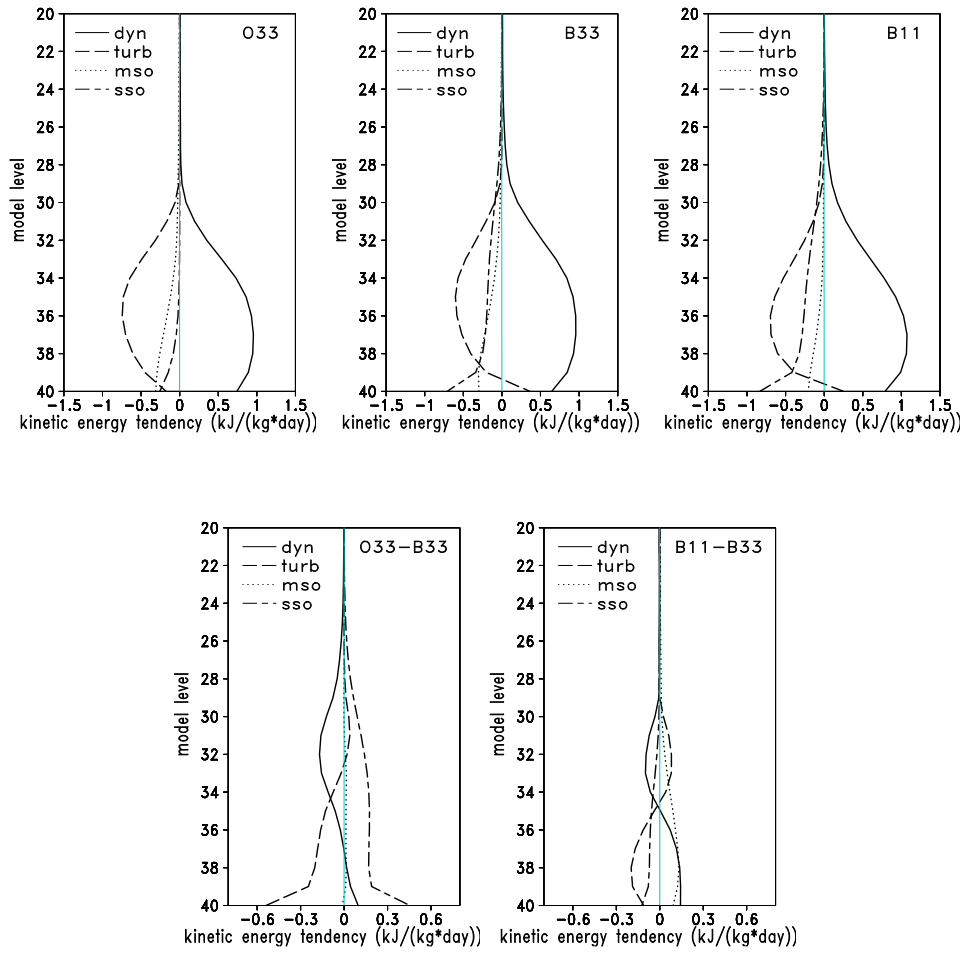
Figure 7. *As Fig. 6, but figures from left to right: O33, B33, B11 (upper row), O33-B33, B11-B33 (lower row).*
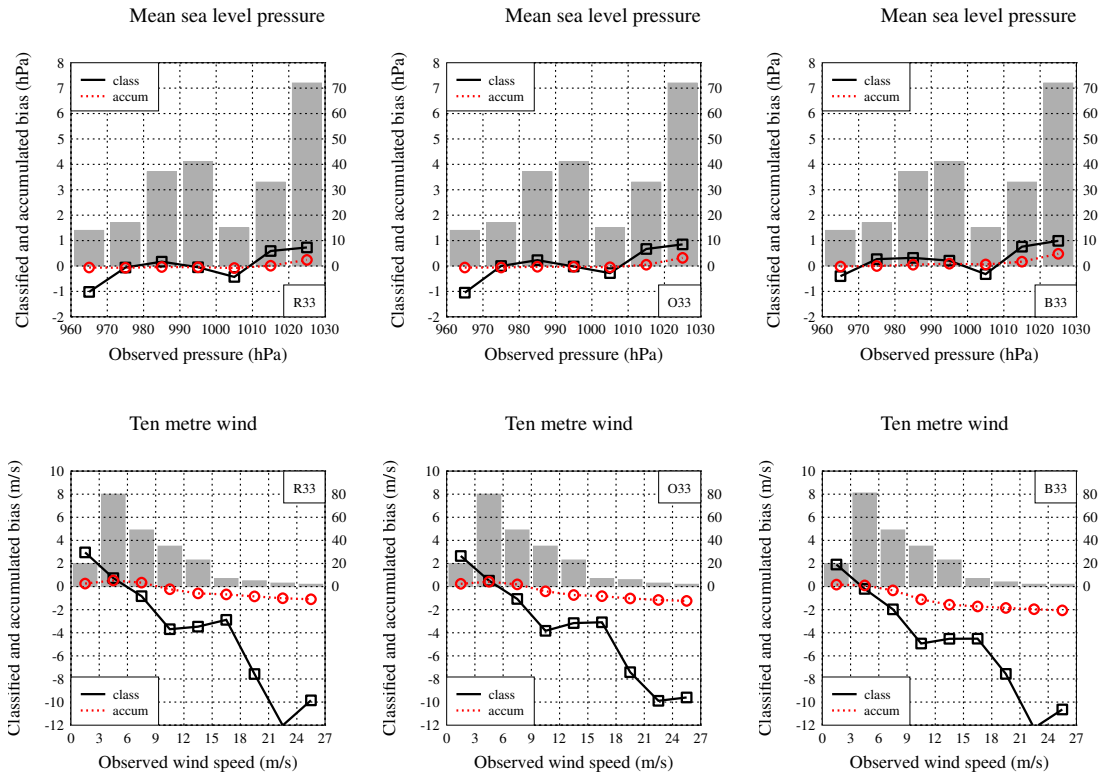
Figure 8. *Systematic difference between predicted and observed (00 UTC + 48h forecast - 00 UTC observation) mean sea level pressure (hPa, upper panel, left y-axis) and ten-metre wind speed (ms^{-1}, lower panel, left y-axis) at the Iceland synoptic stations in January 2000, classified according to observed pressure (hPa, upper panel, x-axis) or wind (ms^{-1}, lower panel, x-axis). Number of observations in each class is shown by shaded bars (right y-axes). The lines with squares show the bias of each class. Lines with circles show the accumulated weighted contribution of the classes to the total bias of 00UTC+48h forecasts, which value is thus shown by the rightmost circle of each line. Experiments from left to right: R33, O33, B33.*
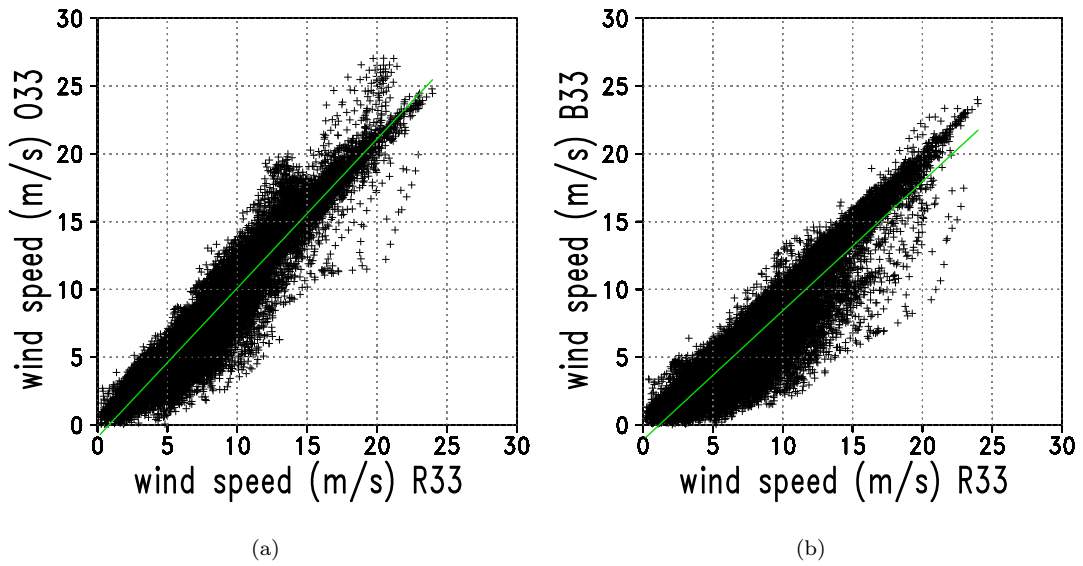

Figure 9. *Magnitude of the lowest model level wind (ms^{-1}) of the experiment O33 (y-axis, a) and B33 (yaxis, b) compared with that of R33 (x-axis, both figures) over Iceland with the open sea grid-points excluded. Based on 31 00UTC+48h forecasts during January 2000. A least squares line is fitted in the scatterplot, with calculated correlations of 0.95 (O33/R33) and 0.92 (B33/R33).*